FUEL DESIGN AND CORE LAYOUT FOR A GAS-COOLED FAST REACTOR

FISSION REACTORS

KEYWORDS: *gas-cooled fast reactor, sustainable nuclear power system, integral fuel cycle*

W. F. G. VAN ROOIJEN,* J. L. KLOOSTERMAN,
T. H. J. J. VAN DER HAGEN, and H. VAN DAM *Delft University of Technology*
Interfacultair Reactor Instituut, Mekelweg 15, 2629 JB Delft, The Netherlands

Received August 27, 2004
Accepted for Publication January 13, 2005

The gas-cooled fast reactor (GCFR) is regarded as the primary candidate for a future sustainable nuclear power system. In this paper a general core layout is presented for a 2400-MW(thermal) GCFR. Two fuel elements are discussed: a TRISO-based coated particle and the innovative hollow sphere concept. Sustainability calls for recycling of all minor actinides (MAs) in the core and a breeding gain close to unity. A fuel cycle is designed allowing operation over a long period, requiring refueling with ^{238}U only. The evolution of nuclides in the GCFR core is calculated using the SCALE system (one-dimensional and three-dimensional). Calculations were done over multiple irradiation cycles including reprocessing. The result is that it is possible to design a fuel and GCFR core with a breeding gain around unity, with recycling of all MAs from cycle to cycle. The burnup reactivity swing is small, improving safety. After several fuel batches an equilibrium core is reached. MA loading in the core remains limited, and the fuel temperature coefficient is always negative.

I. HISTORIC BACKGROUND AND RENEWED INTEREST

The gas-cooled fast reactor (GCFR) is one of the six Generation IV nuclear reactor concepts that is attracting an increasing amount of attention worldwide. Within this framework we investigated a GCFR core layout and fuel design, focusing on high-temperature operation with coated particle (CP) fuel and sustainability. The GCFR concept was already investigated in the 1960s and 1970s in the United States, Japan, the former Soviet Union, and Europe. Early GCFR designs were based on the pin-type liquid metal fast breeder reactor (LMFBR), with a gaseous coolant replacing the liquid metal. One of the principal interests was the reduction of parasitic absorption and moderation by the coolant, resulting in a harder neutron spectrum, improving the breeding gain. All designs used a gas coolant under high pressure (5 to 12 MPa) and a prestressed concrete reactor vessel.

General Atomics (United States)[1,2] presented a detailed design for a GCFR with helium coolant and pin-type fuel with stainless steel cladding. The core consists of a driver fuel zone containing highly enriched fissile material with radial and axial blankets. Mochizuki et al.[3] prepared a design for a GCFR with fuel pins with stainless steel cladding and helium coolant. This design also has a driver core and blankets. In the former Soviet Union, a GCFR was developed using dissociative cooling[1,4,5]: A liquid (N_2O_4) dissociates in the core and recombines to N_2O_4 in the cold leg, releasing heat. Special Cr-based dispersion fuel pins were developed for use with the corrosive coolant.[6] In Europe an international association (Gas Breeder Reactor Association) prepared four designs for a GCFR, aptly named Gas Breeder Reactor (GBR)-1 through GBR-4 (Refs. 7 and 8). These designs featured both helium and CO_2 coolant, and pin-type fuel as well as CP fuel. The GBR-2 and GBR-3 reactors had elevated outlet temperatures (700°C for GBR-2 and 650°C for GBR-3) for improved system efficiency. To accommodate these temperatures CP fuel was required. GBR-2 used helium, and GBR-3 used CO_2 gas. Several problems, including fabrication problems of the required ceramic parts, led to the development of GBR-4, which was a less ambitious design with pin-type fuel, stainless steel cladding, helium coolant, and conventional coolant exit temperature. The temperature reduction allowed the use of steel in the core, while the loss in efficiency was offset by a larger power output of the core. All GBR designs featured a U/Pu driver core and uranium blankets.

The main advantages of the GCFR were thought to be reduced parasitic absorption by the coolant, better chemical compatibility between coolant and cladding, and the impossibility of violent chemical reactions between the coolant and air and water under accidental

*E-mail: rooijen@iri.tudelft.nl

conditions (e.g., sodium reacts violently with both air and water). Fuel economy called for high power density. This, together with the absence of thermal inertia in the core, required a decay heat removal (DHR) strategy with many active backup pumps and pressure holders to ensure adequate cooling under accidental conditions. The worst accident for a GCFR is a depressurization, when all coolant is lost from the primary system. Even with active safety systems, the safety case of GCFRs remained problematic, especially for depressurization accidents.[9] It seems that the problematic DHR behavior and the lack of market demand for the GCFR led to an abandonment of the GCFR concept from the early 1980s on.

Nowadays, the economic and societal circumstances are changing: Fear of depletion of fossil fuel is replaced by a growing concern about CO_2 pollution, and a replacement for fossil fuels is required. The reserves of uranium are larger, and the consumption rate is lower than predicted, allowing a shift from breeder reactors with a high breeding gain and short doubling time to a design focusing on sustainability, with the goal of a self-sustaining core, i.e., a core that breeds just enough new fissile material that refueling with a fertile material only is sufficient. Within the Generation IV framework,[10] the design choices for GCFR differ from the previous GCFR concepts, with the main focus now being on sustainability, and as such, the GCFR is the first nuclear reactor concept to explicitly select sustainability as a primary design goal. The GCFR concept contributes to sustainable development in several ways: by reducing stockpiles of depleted uranium, by optimizing fuel efficiency, and by transmutation of transuranic (TRU) material. The GCFR can produce electricity at high efficiency, or it can be used for CO_2-free hydrogen production.

This paper addresses some basic design choices in Secs. II and III. In Secs. IV and V, the fuel elements and fuel assemblies are presented, and in Sec. VI, the core design is given. The calculation scheme is presented in Sec. VII, followed by the results in Secs. VIII and IX.

II. DESIGN CHOICES FOR THE GCFR

The goal of sustainability is achieved through several design choices. The GCFR uses a closed fuel cycle in which all TRUs are recycled, requiring refueling with ^{238}U or some other fertile material only. Cometto et al.[11] have shown that such a fuel cycle scenario improves the utilization of uranium by a factor of 160 compared to a strategy using only thermal light water reactor (LWR) systems. Hoffman and Stacey[12] show that depleted uranium (the tails of the enrichment process) will become the dominant contribution to the overall radiotoxicity of all materials discharged to the repository from today's nuclear fuel cycle (timescale: 10^5 yr). By converting ^{238}U to ^{239}Pu and subsequent fission, one is left with fission products, most of which have much shorter half-lives than the radioisotopes in the ^{238}U decay chain, thereby reducing the long-term footprint of today's use of nuclear energy. For the GCFR a reprocessing strategy is envisaged with separation of the spent fuel into a stream of fission products and a stream of all actinides. Only the fission products, which have relatively short half-lives, are discharged from the fuel cycle into the repository. Proliferation resistance is increased because there is no separation of Pu in reprocessing. Fertile blankets are avoided, enhancing the proliferation resistance of the GCFR fuel.

The coolant is helium at an inlet temperature of 450°C, a mixed outlet temperature of 850°C, and a pressure between 7 and 10 MPa. Higher system pressure improves economy but worsens the effects of a depressurization accident. Direct cycle electricity production at high efficiency is the primary target with high-temperature heat applications such as thermochemical hydrogen production as a secondary target. The thermal power of the GCFR has not yet been determined, but research focuses on a small unit with a thermal output of 600 MW(thermal) and a large-scale system with an output of 2400 MW(thermal) (Ref. 10). The power density of the system is determined by safety constraints, in particular, DHR in case of depressurization accidents; economic factors (minimization of fuel inventory and compactness of primary system); and sustainability (minimization of fuel needs for long-term deployment). Safety calls for low power density, while the other factors improve with higher power density. The tentative range set by the Generation IV International Forum in Ref. 10 is a power density between 50 and 100 MW/m^3, requiring a minimal coolant fraction in the core of 40%. GCFR power density is lower than in LWRs/pressurized water reactors (PWRs) and much lower than in conventional LMFBRs (300 to 400 MW/m^3). However, it is much higher than with other gas-cooled reactors, such as the High-Temperature Reactor (HTR) or Pebble Bed Modular Reactor (PBMR) (3 to 10 MW/m^3). The total amount of Pu in the fuel cycle is limited to 15 tonnes Pu/GW(electric) (Ref. 10).

III. FUEL AND CORE DESIGN

The temperatures in the GCFR core require a fully ceramic core. To obtain adequate breeding behavior without the use of fertile blankets, the fissile enrichment should be rather low. This leads to a constraint on the minimum volume fraction of fuel in the core to obtain a critical system. Together with the required minimum volume fraction of coolant, the tentative volume fractions in the GCFR core are 40 to 50% coolant; 10% structural materials; 25% fuel; and 25% other materials, such as matrix material or cladding. The specific power (power per unit mass of fissile material) is kept low because of the

combination of low volumetric power density and large fuel volume fraction. Some typical numbers are HTR, 1.2 kW/g fissile; PWR, 1 kW/g fissile; and GCFR, 0.1 to 0.3 kW/g fissile.

There are basically three possibilities for the GCFR basic core type:

1. CP fuel, with or without a binding matrix
2. pin-type fuel with ceramic cladding
3. dispersion fuels based on ceramics (small particles of UPuC or UPuN embedded in SiC, TiC or TiN, or a comparable material).

The fuel volume fraction in the core of a GCFR is relatively low compared to an LMFBR. To obtain an adequate density of heavy metal (HM) in the core, carbide or nitride fuels are used. For the research presented in this paper, nitride fuel has been used because of ease of reprocessing and superior thermal behavior. To avoid ^{14}C production through the $^{14}N(n,p)^{14}C$ reaction, enrichment to 99.9% ^{15}N is required (natural abundance 0.37%). The economic feasibility of such enrichment is still a matter of debate.[13]

TRISO CP fuel has been used very successfully in thermal HTRs, and it is currently the reference fuel form for operating HTRs [High Temperature Engineering Test Reactor (HTTR) and HTR-10] and HTRs under study [PBMR, Gas Turbine Modular Helium Reactor (GT-MHR), Gas Turbine HTR (GTHTR), and Next Generation Nuclear Plant (NGNP)], whereas the other two fuel concepts are completely new. Therefore, it was decided to use TRISO CP fuel as the basis for the GCFR fuel design presented in this paper, although a redesign of the TRISO particle is necessary to adapt the HTR-type fuel particle for GCFR application. Two redesigned coated fuel particles are presented in this paper: a small particle (typical diameter: 1 mm), similar to TRISO CPs, and a hollow fuel sphere [hollow sphere (HS)], an innovative design featuring a hollow shell of fuel surrounded by cladding, with a typical diameter of 3 cm.

IV. FUEL DESIGN

A TRISO CP is made of a spherical fuel kernel (typical diameter: 500 μm), surrounded by a buffer of porous graphite, a layer of pyrolytic carbon [inner pyrolytic carbon (IPyC)], a dense SiC sealing layer, and an outer layer of pyrolytic carbon (OPyC). The buffer provides voidage to accommodate kernel swelling and fission gas release during irradiation and protects the cladding layers from recoiling fission fragments. The SiC layer is the main fission product release barrier and acts as a pressure vessel. The stress induced by a pressure difference ΔP over a thin shell of radius R and thickness δ can be approximated if $\delta \ll R$ (thin shell approximation):

$$\sigma_{xx} = \sigma_{yy} = \frac{R}{2\delta} \cdot \Delta P \quad . \tag{1}$$

This stress σ_{xx} should not exceed the maximum stress σ_{max} of the shell material to avoid failure. An estimate of the pressure in the buffer P_{buf} can be made using the ideal gas law as a first approximation:

$$P_{buf} = \frac{\text{FIMA} \cdot n_0 \cdot z \cdot k \cdot T_{buf}}{V_{buf}} \quad , \tag{2}$$

where

FIMA = fissions per initial metal atom

n_0 = number of HM atoms in the fuel kernel at beginning of cycle (BOC)

z = number of gas atoms released into the buffer per fissioned metal atom

k = Boltzmann's constant

T_{buf}, V_{buf} = temperature and open volume of the buffer layer, respectively.

Note that V_{buf} is a decreasing function of burnup. The pressure difference over the cladding layer should not exceed the limits of the sealing layer. It can be readily inferred from Eqs. (1) and (2) that a CP with a small buffer and a thin sealing layer cannot be used to high burnups.

The IPyC and OPyC layers contract under irradiation, thereby partly relieving the stress on the SiC layer induced by the increasing pressure of fission gasses and kernel swelling during irradiation. The contraction rate of the pyrolytic carbon layers is roughly proportional to the average neutron energy. In a fast neutron spectrum, the layers will contract too quickly and debond from the SiC layer, which leads to failure of the entire particle. Therefore, the IPyc and OPyC layers are removed from the design, and the material of the sealing layer is replaced by ZrC, which is more easily soluble than SiC and chemically more stable at high temperature. The Zr nuclei are more massive than Si nuclei, so damage (atom displacement) induced by collisions with high-energy neutrons will be less severe. A large volume fraction of fuel is required in the particle for GCFR application.

All these considerations together lead to a revised design of the TRISO particle. The GCFR coated fuel particle has a large fuel kernel, a small buffer of porous graphite, and one thin sealing layer of ZrC. Some typical figures for contemporary HTR TRISO design and an envisaged GCFR particle are given in Table I. The ratio of buffer volume to kernel volume of the particles reflects the burnup targets. Values presented in Table I are taken from Verfondern et al.[14] for HTTR, Tang et al.[15] for HTR-10, and from the HTR-N burnup benchmark analysis.[16] The GCFR CP has a small buffer and relatively thin sealing layer (no IPyC/OPyC available to support the

TABLE I

Geometry of Contemporary TRISO Designs

Reactor	HTTR	HTR-10	HTR-N	GCFR
Design FIMA	3%	8%	80%	—
Kernel radius, r_k (μm)	300	249	120	350 to 380
Buffer thickness, t_b (μm)	60	95	95	100 to 70
IPyC thickness, t_{IPyC} (μm)	30	42	40	n/a
SiC thickness, t_{SiC} (μm)	25	37	35	50
OPyC thickness, t_{OPyC} (μm)	45	42	40	n/a
Total radius, r_t (μm)	460	465	330	500
Relative buffer volume, V_{buf}/V_{kernel}	0.73	1.63	4.75	0.66 to 1.13

sealing layer), so the maximum burnup will be limited to several percent. The temperature limits for the CPs are the same as for HTR TRISOs, i.e., maximum operating temperature 1200°C and fission product retention up to 1600°C.

In pebble bed reactors many TRISOs are combined with graphite to make large fuel pebbles. This configuration leads to a temperature difference ΔT_p between the center and the surface of the pebble proportional to the power produced:

$$\Delta T_p = \frac{Q_p}{8\pi\lambda r_{fz}} \quad , \tag{3}$$

where

Q_p = power produced by the pebble (uniform power distribution within the pebble is assumed)

λ = heat conductivity of the graphite mixture

r_{fz} = radius of the fuel zone.

For graphite pebbles in HTRs, ΔT_p can reach values of 300°C. The GCFR requires a larger power density and thus larger Q_p than an HTR, and this, together with the required maximum coolant temperatures, leads to an unacceptably high centerline temperature of the fuel element.

Application of a fuel compact of a different design is also problematic: The random close packing of spheres is ~63%, and the volume fraction of fuel inside a CP is $(r_k/r_t)^3$, with r_k the radius of the fuel kernel and r_t the radius of the entire TRISO particle. To make a fuel compact with CPs and a matrix that satisfies the requirement of containing >45% of fuel by volume requires a CP with a very large kernel and almost no buffer and cladding. When using CP fuel, direct cooling, i.e., a bed of particles with the coolant flowing between the particles, seems to be the most viable solution. An extra advantage is that the temperature differences between the fuel and the coolant remain small.

The amount of voidage available in a CP is determined by the porosity of the buffer layer, which is usually ~50% for TRISO CPs. Removing all material in the buffer layer creates more empty space to accommodate kernel swelling and fission gas storage. This observation has led to the design of the HS innovative fuel particle. The HS is a hollow shell of fuel material with ceramic cladding around it (Fig. 1). It is comparable to the fuel element proposed by Ryu and Sekimoto[17] for GCFR applications.

Recoiling fission fragments will penetrate the cladding, but this should be no problem as long as the cladding thickness is much larger than the penetration depth of the fission fragments (typically several micrometers). An HS could be manufactured by pressing a mixture of fuel powder with a gelating agent to form hollow hemispheres. Two hemispheres are attached to each other and then sintered to form a full sphere, onto which a thick ceramic cladding layer is deposited. The sintering step takes place at high temperature. The amount of gas within the void should be controlled during sintering. Doing so, the HS will be under compressive stress at room temperature (gas contracted), while at operating temperature the overpressure inside the void remains limited. In a hollow

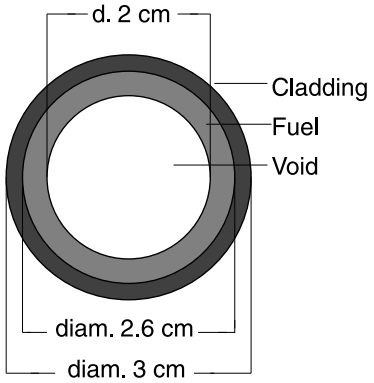

Fig. 1. A cross-sectional view of the HS fuel element. The entire central void is available to accommodate fuel swelling and fission gas release.

fuel sphere, the inner void is completely empty, providing more voidage than a TRISO CP with the same volume fraction of fuel and cladding. An HS with the same volume fractions of fuel and cladding as a TRISO CP has more space to store fission products and contains less moderating material, reducing parasitic absorption and yielding a harder neutron spectrum.

Both fuel elements presented in this paper offer many parameters that can be tuned to optimize the fuel design. For instance, the volume fractions of fuel, buffer, and cladding can be varied.

V. PRESSURE DROP OVER PACKED BEDS OF SPHERES

In our design the fuel elements are cooled directly by helium. The coolant flow through the packed bed causes a pressure drop ΔP_{pb}, which drop should not exceed ~2% of the system pressure in order to limit the required pumping power.[18] It is necessary to find an expression to estimate the largest allowable height of the packed bed of fuel spheres. ΔP_{pb} can be estimated using the Ergun-relation[19]:

$$\frac{\Delta P_{pb}}{L} = 150 \frac{(1-\epsilon)^2}{\epsilon^3} \frac{\mu_f}{d_p^2} u + 1.75 \frac{1-\epsilon}{\epsilon^3} \frac{\rho_f}{d_p} u^2 \quad , \quad (4)$$

where

L = bed height

ϵ = porosity of the bed

μ_f = viscosity of the fluid

d_p = diameter of the spherical particles

u = superficial fluid velocity

ρ_f = density of the fluid.

The superficial velocity is proportional to the mass flow rate $\dot{m}$:

$$\dot{m} = \rho_f A u \quad , \quad (5)$$

where A is the cross-sectional flow area. The mass flow rate required to remove the heat from a packed bed of power-producing spheres is proportional to the volume of the bed multiplied by the average power density of the bed $\bar{Q}$:

$$\dot{m} = \frac{\bar{Q} L A}{c_p \Delta T} \quad , \quad (6)$$

where

ΔT = temperature rise over the bed of spheres

c_p = isobaric heat capacity of the fluid.

It is assumed that the pressure drop over the bed is small compared to the system pressure, so that c_p can be taken as a constant. Combining the Eqs. (4), (5), and (6) leads to a revised expression for the Ergun relation:

$$\Delta P_{pb} = 150 \frac{(1-\epsilon)^2}{\epsilon^3} \frac{\mu_f}{\rho_f d_p^2} \frac{\bar{Q} L^2}{\Delta T c_p} + 1.75 \frac{1-\epsilon}{\epsilon^3} \frac{1}{\rho_f d_p} \frac{\bar{Q}^2 L^3}{\Delta T^2 c_p^2} \quad . \quad (7)$$

This alternative version of the Ergun relation can be used to estimate the pressure drop over a bed of power producing spheres with a given volumetric power density using a given coolant at given temperature and pressure. For a core with $\bar{Q}$ = 50 MW/m^3, L = 7.5 cm, ϵ = 0.37, ΔT = 400°C, T_{out} = 850°C, and a particle diameter of 1 mm, Eq. (7) gives ΔP_{pb} = 0.04 bar, while for a particle diameter of 3 cm and a bed height of 50 cm, Eq. (7) gives 0.15 bar.

VI. OVERALL CORE LAYOUT

Using the results of Secs. IV and V, a core design can be made:

1. With ΔT fixed, the pressure drop increases with increasing power density, favoring a low power density (with the additional advantage of reduced pumping power and DHR by natural circulation).

2. The relatively low volume fraction of fuel in the spherical fuel elements with the constraint of a low fissile enrichment favors a large core to reduce leakage.

It was decided to prepare a core layout for a GCFR with 2400-MW(thermal) output, an average power density of 50 MW/m^3, a height h_c of 3 m, and a radius r_c of 2.25 m, with stainless steel reflectors. The fuel is made of ^{238}U and recycled LWR Pu. The Pu vector is taken from the HTR-N burnup benchmark[16] and given by

$$^{238}\text{Pu}/^{239}\text{Pu}/^{240}\text{Pu}/^{241}\text{Pu}/^{242}\text{Pu} = 1/62/24/8/5\% \quad .$$

There are three enrichment zones in the core, chosen to give a reasonably flat power profile at start-up. The specific power (W/g fissile) is rather low for the GCFR, leading to long irradiation periods. For the simulations presented here, one cycle takes 1900 days, resulting in a burnup of ~4 to 5% FIMA, depending on initial fuel loading. The temperature of the inlet and the outlet are 450 and 850°C, respectively, and the system pressure is 7 MPa. Using $\bar{Q}$ = 50 MW/m^3 and using the properties of helium ρ_f, μ_f at an average temperature of 650°C, and c_p = 5.2 J/g·K^{-1} (Ref. 18), the pressure drop can be calculated for a given geometry of the fuel bed and the fuel particles. For CPs with a diameter of 1 mm, the maximum allowable bed height is only several centimeters, and for HSs with a diameter of 3 cm, the maximum bed height is just several tens of centimeters.

The maximum allowable bed height for both types of fuel spheres precludes the use of a pebble bed configuration as used in the PBMR or Thorium HTR (THTR). Instead, an approach with annular cylinders is taken: The fuel spheres are located in annular cylinders, with the coolant flowing radially through the beds of fuel spheres.

VI.A. Core with CP fuel

For CPs a fuel cylinder is made up of two perforated concentric annuli, with the CPs sandwiched between the perforated annuli (Fig. 2).

The height of the cylinder is h_c, while the particle bed thickness is ~2.5 cm. The overall diameter of such a fuel cylinder would be ~10 to 15 cm. The coolant enters the cylinder at the bottom and exits at the top. The coolant flows inward to keep a compressive stress on the perforated cylinders. All parts are ceramics. The highest fluid velocities will occur at the outlet and the inlet. The maximum allowable fluid velocity determines the minimum areas of the inlet and the outlet, and this also puts a maximum on the volume fraction that the fuel beds can occupy in the cylinder. The fuel beds occupy 75% of the cylinder volume. The fuel cylinders are arranged in a hexagonal lattice in the core. The overall core volume fraction of the coolant equals 57%, the volume fraction of the fuel spheres is 43%, and the fuel volume fraction is $(r_k/r_t)^3 \times 0.43$. If annular hexagons are used instead of annular cylinders, the overall coolant volume fraction decreases, and the fuel fraction may increase. The presented fuel cylinder concept is comparable to that presented by Chermanne in Ref. 7. With a lower h_c the volume of the fuel cylinder is reduced, allowing for a larger fraction of CPs with the same power density, or a larger power density with the same fraction of CPs. An example of a GCFR core with low h_c and high power density is presented by Konomura et al. in Ref. 20.

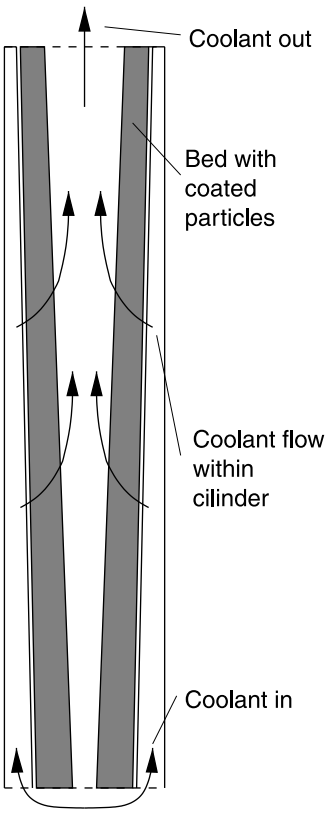

Fig. 2. Annular fuel cylinder. The coolant enters at the bottom, flows inward through the packed bed of fuel particles (gray area), and exits at the top. The inward flow assures a compressive stress on the inner cylinder. The fuel bed is conical.

VI.B. Core with Hollow Fuel Spheres

The HS concept allows a larger bed height. The reactor core is divided into three concentric rings of fuel spheres, with the coolant entering between the beds. The coolant then flows through the beds and exits the reactor (Fig. 3). The height of the beds in the axial direction is h_c; in the radial direction it is ~50 cm. Again, the highest fluid velocities occur at the inlet and the exit. The maximum coolant velocity determines the minimum dimensions of

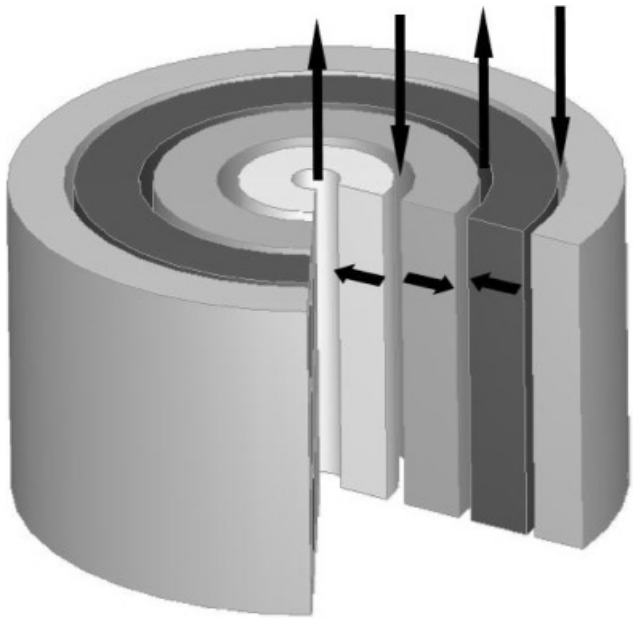

Fig. 3. An illustration of the core with hollow fuel spheres. From the inside out the white, light-gray and dark-gray areas are the three fuel beds, each with a different initial enrichment. The outer light-gray area is the radial reflector. The top and bottom reflectors are not shown. The empty spaces are for the coolant flow. The coolant flow is indicated by the arrows.

the nonfuel areas, and thus, the overall maximum volume fraction of HSs is limited.

VII. CALCULATIONS

One-dimensional (1-D) calculations were done to roughly estimate reactor parameters (k_{eff} and fuel vector evolution) and to make a fuel design. Three-dimensional (3-D) calculations were done to give more accurate results for k_{eff} and fuel evolution and to have the possibility of including axial reflectors and a more realistic temperature profile. Simulations where done using various modules of the SCALE 4.4a code system,[21] interconnected by a Perl script and some in-house Fortran codes. A JEF-2.2 172-group AMPX library was used for cross-section processing.[22] For the CPs the simulation assumes a hexagonal lattice of fuel particles. Each CP is surrounded by coolant, such that the volume fractions of fuel, cladding, and coolant in the unit cell correspond to the core average values. This lattice does not correspond to the actual (stochastic) lattice, but the errors will be small as the mean free path of a neutron in the GCFR is large compared to the size of a unit cell. For the HS fuel the reactor is subdivided into fueled and nonfueled regions. In the fueled parts the fuel is simulated as a hexagonal lattice of fuel spheres. The volume fractions in the unit cell are the average values of the fuel bed (i.e., 37% coolant).

With regard to 1-D calculations, for each individual fuel region, CSAS1X (BONAMI–NITAWL–XSDRNPM) is used to determine cell-weighted cross sections, and an extra XSDRNPM calculation is done to obtain the zone-weighted (i.e., nonhomogenized) cross sections. The homogenized cross sections are then used in a 1-D XSDRNPM calculation over the entire reactor, with an axial buckling to account for the finite height of the reactor. The k_{eff} and the flux profile in the entire reactor are determined. The power profile is calculated from the flux profile and the mixture cross sections, including the reflectors (energy release from inelastic scattering is taken into account). The power profile and zone-weighted cross sections are used to calculate the fuel depletion (COUPLE–ORIGEN-S) in each fuel region. Because of the 1-D calculation, only concentric fuel zones can be used, and there is no axial dependence of the fuel depletion.

With regard to 3-D calculations, CSASIX (BONAMI–NITAWL–XSDRNPM–ICE) is used to obtain homogenized cross sections for each mixture defined in the reactor. Nonfuel mixtures are treated as well. An extra XSDRNPM calculation is used to obtain nonhomogenized cross sections for each mixture containing fuel. KENOV is used to determine k_{eff} and the flux profile of the entire reactor. The power profile is calculated using the flux profile and mixture cross sections. The power profile and nonhomogenized cross sections are used to calculate the fuel depletion (COUPLE–ORIGEN-S). The simulations done for this paper are essentially *R-Z*–type calculations, but a full 3-D geometry can be simulated.

The fuel temperature coefficient (FTC) was calculated by performing a spectrum calculation at $T_0 + \Delta T_0$, followed by a determination of $k_{eff}(T_0 + \Delta T_0)$. The FTC is calculated using

$$\text{FTC} = \frac{k(T_0 + \Delta T_0) - k(T_0)}{k(T_0)} \cdot \frac{1}{\Delta T_0}$$

and expressed in pcm/°C, with $\Delta T_0 = 100$°C for 1-D calculations. For the 3-D case $\Delta T_0 = 200$°C because KENO gives a confidence interval for k_{eff} and these intervals should not overlap for an accurate FTC. Simulations include reprocessing, where it is assumed that all minor actinides (MAs) are recycled and only ^{238}U is added to give the same amount of fuel as the first core. The differences in Pu content per zone are maintained. One irradiation cycle takes 1900 days, and the fuel is allowed to cool down and decay for another 1900 days after irradiation (ORIGEN-S is used to calculate the resulting fuel vector). The new fuel composition is then calculated and irradiated for a new period.

VIII. RESULTS

For both the CP and HS concepts, two fuel compositions were made using 1-D calculations: one fuel composition with low and one with high Pu fraction. The fuel composition is such that the initial HM loading is roughly the same for the CP and the HS cores, and such that the k_{eff}'s of the cores are roughly the same at fresh start-up. In the design with low Pu fraction, the HS core becomes critical with a slightly lower initial enrichment than the CP core (13.4% for the CP and 12.5% for the HS core). This is attributed to the fact that the CP core has more nonfuel material in the core (the buffer material) giving slightly more absorption and a softer spectrum. Under the assumption of a 50% efficient power conversion system, the GCFR will have 1200-MW(electric) output. The low Pu cores contain 15.7 tonnes Pu (CPs) and 14.3 tonnes Pu (HS), so they are close to but within the tentative maximum of 15 tonnes Pu/GW(electric). Both cores have a k_{eff} just above 1 at start-up.

The high Pu cores have a lower HM loading than the low Pu cores; otherwise, k_{eff} would become very large because of high fissile content. The high Pu cores in fact contain a smaller total mass of Pu than the low Pu cores ($\sim$13.5 tonnes Pu). The difference in k_{eff} at BOC of the low Pu CP core and the high Pu CP core is negligible, but for the HS core, there is some difference in k_{eff} between the high and low Pu versions. The different HM loading (see Table II) is achieved for the CP core by using a smaller fuel kernel. The outer radii of the buffer and the cladding are kept constant, so the volume of the buffer is larger for the CPs with a smaller kernel. The larger buffer

TABLE II

Results of the Burnup Study for the CP Core*

Results for CP Core		
	Low Pu Content	High Pu Content
Batch 1		
HM total (kg)	117 379	91 725
Percentage of which is Pu (kg)	15 733/13.4%	13 830/15.1%
$^{238}Pu/^{239}Pu$	1%/62%	1%/62%
$^{240}Pu/^{241}Pu/^{242}Pu$	24%/8%/5%	24%/8%/5%
$\Delta Pu/\Delta Pu_{fissile}$	+2.2%/−0.7%	−0.7%/−6.1%
EOC MA mass (kg)	514	592
k_{max}/k_{min}	1.0651/1.0491	1.0658/1.0116
FTC_{max}/FTC_{min} (pcm/K)	−2.07/−1.42	−2.6/−1.5
Batch 2		
HM total (kg)	117 387	91 731
Percentage of which is Pu (kg)	16 083/13.8%	13 728/15%
$^{238}Pu/^{239}Pu$	0.85%/63.7%	0.87%/61.7%
$^{240}Pu/^{241}Pu/^{242}Pu$	26.3%/4.3%/4.9%	27.9%/4.4%/5.1%
$\Delta Pu/\Delta Pu_{fissile}$	+3.7%/+1.3%	+2.0%/−2.1%
EOC MA mass (kg)	734	850
$k_{max/k_{min}}$	1.0449/1.0333	1.0045/0.9941
FTC_{max}/FTC_{min} (pcm/K)	−1.79/−1.48	−2.5/−1.3
Batch 3		
HM total (kg)	117 392	91 736
Percentage of which is Pu (kg)	16 672/14.3%	14 002/15.4%
$^{238}Pu/^{239}Pu$	1.1%/63.4%	1.2%/60.0%
$^{240}Pu/^{241}Pu/^{242}Pu$	27.9%/3.1%/4.6%	30.4%/3.5%/4.8%
$\Delta Pu/\Delta Pu_{fissile}$	+3.3%/+1.3%	+2.3%/−0.7%
EOC MA mass (kg)	851	994
k_{max}/k_{min}	1.0521/1.0360	0.9910/0.9959
FTC_{max}/FTC_{min} (pcm/K)	−1.88/−1.33	−3.0/−0.96
Batch 4		
HM total (kg)	117 397	91 740
Percentage of which is Pu (kg)	17 230/14.8%	14 329/15.7%
$^{238}Pu/^{239}Pu$	1.4%/62.4%	1.5%/58.3%
$^{240}Pu/^{241}Pu/^{242}Pu$	29.2%/2.7%/4.3%	32.2%/3.4%/4.6%
$\Delta Pu/\Delta Pu_{fissile}$	+2.7%/+1.0%	+2.1%/−0.2%
EOC MA mass (kg)	930	1096
k_{max}/k_{min}	1.0594/1.04396	0.9891/0.9972
FTC_{max}/FTC_{min} (pcm/K)	−1.77/−1.33	−2.2/−1.3
Geometry of the Fuel Element		
Kernel radius, r_k (μm)	380	350
Buffer radius, r_b (μm)	450	450
Cladding radius, r_c (μm)	500	500

*All MAs are recycled; ^{238}U is added after each batch.

volume also means that some of the extra reactivity of the high Pu fuel is lost by extra absorption in the buffer material. For the HS core the thickness of the fuel shell is varied. A smaller fuel shell means a larger central void.

The 1-D calculations show that both cores have a negative FTC and that the magnitude of the FTC decreases slightly during irradiation. The decrease is caused by the hardening of the spectrum due to fission product buildup during irradiation. In Fig. 4 the flux per unit lethargy is given at 0 and 1900 days of irradiation, together with the resonances of σ_a of ^{238}U. Note the decreased flux in the resonance region after 1900 days of irradiation.

The 1-D calculations show that the high Pu cores have a net consumption of fissile Pu over the first irradiation cycle. The low Pu cores have a net increase in fissile mass during irradiation, but during the subsequent decay period, some of the ^{241}Pu decays. The HS core with low Pu loading has a net increase of fissile mass, and the CP core has a slight decrease in fissile mass after decay. Overall, the low Pu cores have more conversion, which is as expected (more ^{238}U nuclei to absorb neutrons). Comparing the evolution of the nuclide densities in the cores, there is not much difference between the CP and HS cores. This applies for Pu as well as for the MAs. Apparently, the influence of the buffer material is not big enough to cause large spectral changes. In all cores there is a noticeable consumption of ^{241}Pu, offset by a net production of ^{239}Pu in the low Pu cores. In the high Pu cores, there is a net consumption of ^{239}Pu.

A 3-D calculation including reprocessing was done. An irradiation and subsequent decay period are designated as one batch. A total of four batches was simulated for all core designs. Each batch includes 1900 days of irradiation and 1900 days of decay, so four batches equal a period of 15 200 days (= 41.6 yr). The 3-D calculations include a top and a bottom reflector of stainless steel. A comparison between 1-D and 3-D results of the first batch show that the nuclide evolution is nearly the same, but k_{eff} is consistently higher for the 3-D calculations. Apparently, the top and bottom reflectors have no great spectral influence, but they do reduce leakage and improve k_{eff}. As an example the 1-D and 3-D k_{eff} and FTC of the low Pu CP core are given in Fig. 5, with the corresponding evolution of the Pu density in Fig. 6. Figures 7 and 8 show the same for the HS core with high Pu loading. The 3-D FTC graph is not as smooth as the 1-D FTC, due to the statistical nature of the KENO calculations. The results could be improved, but the required CPU time would increase drastically.

The reprocessing strategy involves recycling of all actinides in the GCFR. This means that the fuel at the beginning of a new batch will contain all MAs that have not decayed during the decay period. In practice, only some isotopes of Am (^{241}Am, ^{242m}Am, ^{243}Am) and Cm (^{243}Cm, ^{244}Cm, ^{245}Cm) are stable enough to be present in the new fuel in appreciable amounts. In Tables II and III, the sum of the masses of Np, Am, and Cm is given at end of cycle (EOC) (one cycle comprises 1900 days of irradiation and 1900 days of decay). Americium-241 is the

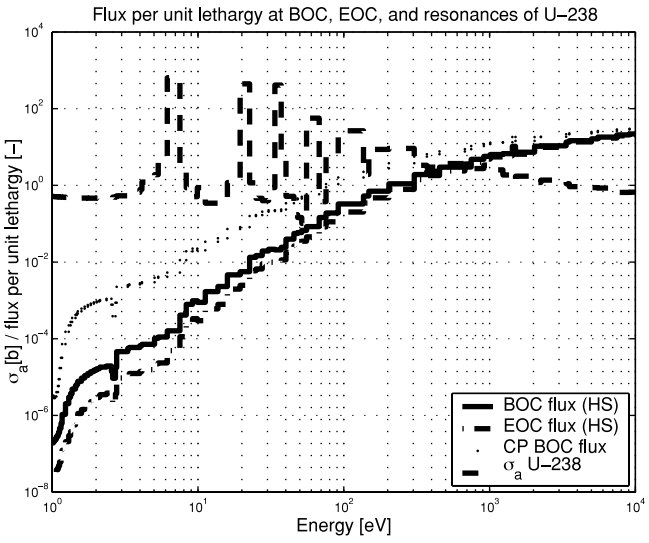

Fig. 4. The flux per unit lethargy as a function of energy after 0 and 1900 days of irradiation in the HS core. The resonances of σ_a of ^{238}U are also shown. After 1900 days the spectrum has hardened, giving a lower flux in the ^{238}U resonances, leading to lower absorption and a decrease in the magnitude of the FTC. The BOC spectrum of the CP core is indicated by dots. This spectrum is softer than the HS spectrum.

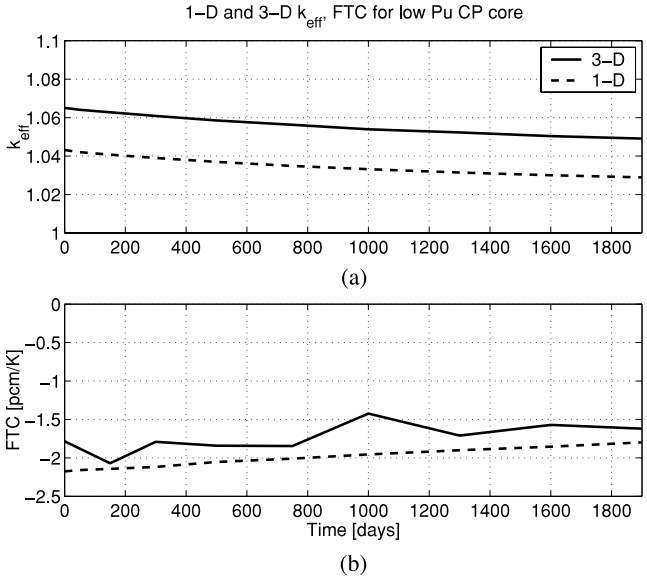

Fig. 5. (a) The k_{eff} of the CP low Pu core as calculated using 1-D and 3-D calculations. (b) The FTC of the CP low Pu core.

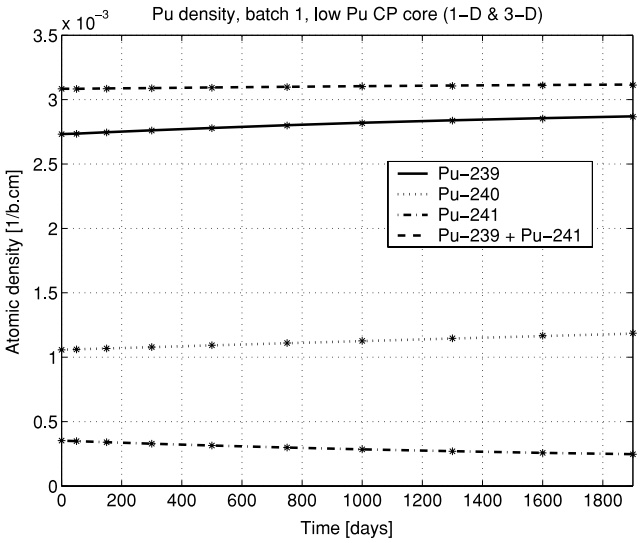

Fig. 6. Evolution of ^{239}Pu, ^{240}Pu, and ^{241}Pu during batch 1 for the CP low Pu core. Lines indicate 3-D results; dots are the 1-D results. The differences between the 1-D and the 3-D results are very small.

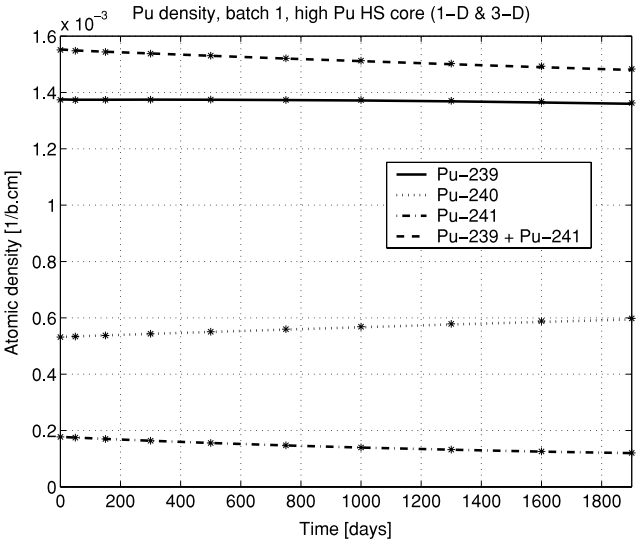

Fig. 8. Evolution of ^{239}Pu, ^{240}Pu, and ^{241}Pu during batch 1 for the HS high Pu core. Lines indicate 3-D results; dots are 1-D. The differences between the 1-D and the 3-D results are small.

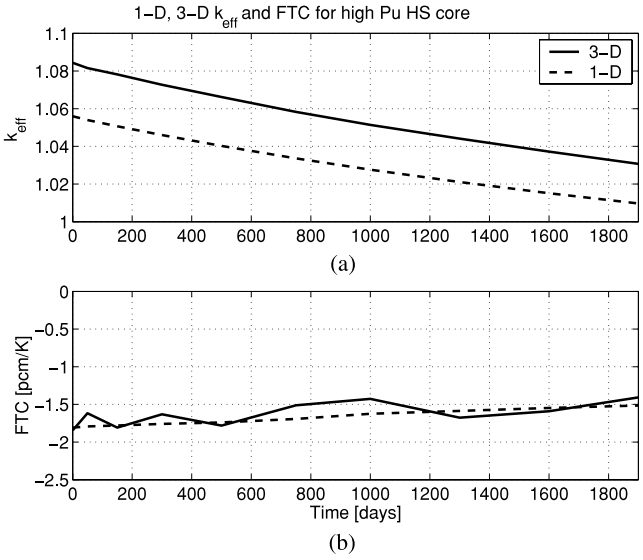

Fig. 7. (a) The k_{eff} of the high Pu HS core calculated using 1-D and 3-D calculations. (b) The FTC of the same core.

decay product of ^{241}Pu. It is the most abundant of the MAs, and it is the only MA whose mass increases during the decay period. During irradiation a net consumption of ^{241}Am occurs, but this is offset by production from ^{241}Pu decay during the decay period. In the first few fuel batches, ^{241}Am production from ^{241}Pu decay is much more than the consumption during irradiation, but this situation changes in the later fuel batches because the higher amount of ^{241}Am in the fuel leads to higher consumption of ^{241}Am.

VIII.A. Results for CPs

The results of the burnup simulation for the CP cores over four fuel batches are summarized in Table II, which gives the initial HM and Pu mass for each fuel batch, as well as the Pu vector at BOC of each batch. The change of the total amount of Pu (^{238}Pu through ^{242}Pu) is given together with the change of fissile Pu (^{239}Pu and ^{241}Pu). The total mass of MA in the core, which is the sum of the masses of ^{237}Np, ^{241}Am, ^{242m}Am, ^{243}Am, ^{243}Cm, ^{244}Cm, and ^{245}Cm at EOC is indicated in Table II. Because of the applied calculation scheme, the MA mass at BOC is equal to the EOC mass of the previous cycle, except for the first batch. Also given are the minimum and maximum values of k_{eff} and FTC. The k_{eff} is not necessarily a monotonically decreasing function of irradiation time, and it seems better to give the minimum and the maximum values of k_{eff} and FTC per batch. After 1900 days of irradiation, the low Pu core reaches a burnup of 3.8% FIMA, and the high Pu core, which has a lower initial HM loading, reaches a burnup of 4.9% FIMA. Using Eq. (2) with $z = 0.8$, the pressure in the buffer at these burnups is estimated between 2 and 4 MPa, so the CPs are still under compression in the reactor.

VIII.A.1. Plutonium Evolution

Note the large increase of ^{240}Pu in both cores and the decrease of ^{241}Pu. The low Pu core has a good conversion of ^{238}U to ^{239}Pu, resulting in a fuel vector with a high amount of ^{239}Pu and ^{240}Pu at the beginning of the last batch. The high Pu core has lower conversion, so the loss of ^{239}Pu and ^{241}Pu is not made up by conversion of

TABLE III

Results of the Burnup Study for the HS Core*

Results for Hollow Fuel Sphere Core		
	Low Pu Content	High Pu Content
Batch 1		
HM total (kg)	114 585	86 144
Percentage of which is Pu (kg)	14 336/12.5%	13 374/15.5%
$^{238}Pu/^{239}Pu$	1%/62%	1%/62%
$^{240}Pu/^{241}Pu/^{242}Pu$	24%/8%/5%	24%/8%/5%
$\Delta Pu/\Delta Pu_{fissile}$	+4.4%/+2.7%	−1.8%/−6.3%
EOC MA mass (kg)	458	427
k_{max}/k_{min}	1.0294/1.0331	1.0844/1.0307
FTC_{max}/FTC_{min} (pcm/K)	−2.3/−1.2	−1.84/−1.41
Batch 2		
HM total (kg)	114 552	86 148
Percentage of which is Pu (kg)	14 960/13.1%	13 131/15.3%
$^{238}Pu/^{239}Pu$	0.8%/64.8%	0.9%/62.5%
$^{240}Pu/^{241}Pu/^{242}Pu$	25.5%/4.1%/4.8%	27.3%/4.3%/5.1%
$\Delta Pu/\Delta Pu_{fissile}$	+4.8%/+3.2%	+1.1%/−2.2%
EOC MA mass (kg)	645	600
k_{max}/k_{min}	1.0396/1.0174	1.0233/1.0128
FTC_{max}/FTC_{min} (pcm/K)	−2.1/−1.2	−1.76/−1.23
Batch 3		
HM total (kg)	114 557	86 151
Percentage of which is Pu (kg)	15 681/13.8%	13 281/15.5%
$^{238}Pu/^{239}Pu$	1%/65%	1.2%/61.3%
$^{240}Pu/^{241}Pu/^{242}Pu$	26.7%/2.8%/4.4%	29.4%/3.2%/4.8%
$\Delta Pu/\Delta Pu_{fissile}$	+3.9%/+2.4%	+1.6%/−0.7%
EOC MA mass (kg)	742	688
k_{max}/k_{min}	1.0516/1.0310	1.0141/1.0100
FTC_{max}/FTC_{min} (pcm/K)	−2.0/−0.7	−1.73/−1.48
Batch 4		
HM total (kg)	114 562	86 154
Percentage of which is Pu (kg)	16 290/14.3%	13 500/15.8%
$^{238}Pu/^{239}Pu$	1.3%/64.3%	1.5%/60%
$^{240}Pu/^{241}Pu/^{242}Pu$	27.8%/2.5%/4.1%	30.9%/3.0%/4.6%
$\Delta Pu/\Delta Pu_{fissile}$	+3.0%/+1.5%	+1.5%/−0.3%
EOC MA mass (kg)	806	746
k_{max}/k_{min}	1.0625/1.0451	1.0153/1.0087
FTC_{max}/FTC_{min} (pcm/K)	−1.8/−0.8	−1.88/−1.28
Geometry of the Fuel Element		
Sphere diameter (cm)	3	3
Cladding thickness (cm)	0.2	0.2
Fuel thickness (cm)	0.325	0.225

*All MAs are recycled; ^{238}U is added after every batch.

^{238}U. The total Pu mass in both the low and high Pu cores grows from batch to batch. Conversion of ^{241}Pu to ^{242}Pu is low and decreases in later batches because of a decreasing ^{241}Pu content.

VIII.A.2. k_{eff}

The high Pu core has quite a big loss of fissile mass during the first and second batches, resulting in a subcritical system in the third and fourth batches. However, an increase of the HM loading would improve the situation, and because the spectrum and geometry of the CP would not change much, the evolution of the nuclides would not be highly affected. This means that the calculations presented here still give valuable results. For the CP fuel the buffer volume is larger for a smaller fuel kernel. Because the buffer contains graphite, moderation and absorption increase with decreasing kernel size. A softer spectrum leads to increased resonance absorption by nonfuel materials in the core, reducing k_{eff}.

VIII.A.3. FTC

The FTC is always negative and shows a decreasing magnitude during burnup.

VIII.A.4. Minor Actinides

The high Pu core produces more MAs than the low Pu core, which is as expected (more Pu available for conversion and a slightly softer spectrum favoring absorption over fission of actinides). Notice that the increase in MA mass gets smaller from batch to batch; e.g., in the first batch of the low Pu CP core, 514 kg of MAs are formed, and in the fourth batch, the EOC amount is only 79 kg more than the EOC mass of batch 3.

VIII.B. Results for HSs

For the HS core the same burnup simulation over four fuel batches was performed. The results are summarized in Table III, which gives for each fuel batch the initial HM and Pu mass, the Pu vector at BOC, the change in Pu mass over the irradiation period, and the change in fissile mass. Also given is the EOC MA mass. The minimum and the maximum values of k_{eff} and FTC are also given. The burnup reached after 1900 days of irradiation equals 4% FIMA for the low Pu HS core and 5.3% FIMA for the high Pu version.

VIII.B.1. Plutonium Evolution and k_{eff}

The HS fuel element has a lower volume fraction of nonfuel material than the CPs because the HS lacks the buffer material. A reduction of the thickness of the fuel shell does not increase the amount of nonfuel materials in the core. This means that the neutron spectrum and absorption are almost unaffected by a change in fuel loading of an individual fuel element. The initial enrichment of the low Pu HS core is almost 1% lower than the low Pu CP core, and k_{eff} is slightly lower than the low Pu CP design. The low Pu content causes a large conversion from ^{238}U to ^{239}Pu. The low Pu HS design shows an increase of the fissile mass for all four fuel batches. Since the total Pu mass also increases from batch to batch, conversion from ^{238}U to ^{239}Pu decreases in the later fuel batches, and although the Pu mass grows quickly initially, the Pu content in the fourth batch is still lower than the initial enrichment of the high Pu core.

The high Pu HS core has a lower HM loading than the high Pu CP core, offset by a higher initial enrichment of the fuel. The magnitude of k_{eff} is comparable for both cores, as is the evolution of Pu in the core during the four batches. The high Pu HS fuel shows a considerable loss of fissile material in the first two fuel batches but remains critical during four batches. At the start of the last batch, the amount of ^{241}Pu has decreased drastically in both cores, while the loss of fissile mass per batch is reduced from 6.3% in the first batch to only 0.3% in the last batch. The high Pu core has a lower production of ^{239}Pu, resulting in a Pu vector that is rich in ^{240}Pu. Conversion of ^{241}Pu to ^{242}Pu is low and decreases in later batches because of a decreasing ^{241}Pu content.

The total Pu mass in the high Pu HS core changes by 0.9% from the first to the fourth batch. In the same period the Pu mass of the high Pu CP core increases by 3.6%. The Pu in the CP core contains more ^{240}Pu than the HS Pu. This is attributed to different initial Pu contents, and the softer spectrum in the CP core; i.e., resonance absorption by ^{239}Pu is enhanced, reducing the fissile mass and k_{eff} while at the same time producing ^{240}Pu. Plutonium-241 (converted from ^{240}Pu) is also slightly higher in the CP core.

VIII.B.2. FTC

FTC is always negative with a decreasing magnitude in the course of the irradiation.

VIII.B.3. Minor Actinides

In comparison to the CP core, the HS core produces a smaller amount of MAs. This can be attributed to less absorption by and more fission of MAs because of the harder neutron spectrum in the HS core (see Fig. 4).

We can draw the conclusion that it is possible to obtain a breeding close to unity. The low Pu CP and high Pu HS core concepts look the most promising because they maintain criticality without too much increase of fissile material.

IX. EXTENDED TIME CALCULATIONS

To examine the long-term evolution of the fuel, a calculation was done over eight fuel batches. Two reactor

configurations were simulated: the CP core with low Pu content and the HS core with high Pu content. In Table IV a short summary of the results is given: the initial Pu content of every batch at BOC, and ΔPu and $\Delta Pu_{fissile}$ per batch from BOC to EOC (which includes reprocessing). Also given is the EOC MA mass for each fuel batch.

TABLE IV

Results of the Burnup Study over Eight Batches

Long-Term Burnup		
	CP Core/ Low Pu	HS Core/ High Pu
Batch 1		
Pu initial	13.4%	15.5%
$\Delta Pu/\Delta Pu_{fissile}$	+2.2%/−0.7%	−1.8%/−6.3%
EOC MA mass (kg)	514	427
Batch 2		
Pu initial	13.8%	15.3%
$\Delta Pu/\Delta Pu_{fissile}$	+3.7%/+1.3%	+1.1%/−2.2%
EOC MA mass (kg)	734	600
Batch 3		
Pu initial	14.3%	15.5%
$\Delta Pu/\Delta Pu_{fissile}$	+3.3%/+1.3%	+1.6%/−0.7%
EOC MA mass (kg)	851	688
Batch 4		
Pu initial	14.8%	15.8%
$\Delta Pu/\Delta Pu_{fissile}$	+2.7%/+1.0%	+1.5%/−0.3%
EOC MA mass (kg)	930	746
Batch 5		
Pu initial	15.2%	16.0%
$\Delta Pu/\Delta Pu_{fissile}$	+2.2%/+0.7%	+1.3%/−0.1%
EOC MA mass (kg)	994	790
Batch 6		
Pu initial	15.5%	16.2%
$\Delta Pu/\Delta Pu_{fissile}$	+1.8%/+0.4%	+1.0%/−0.1%
EOC MA mass (kg)	1047	824
Batch 7		
Pu initial	15.8%	16.4%
$\Delta Pu/\Delta Pu_{fissile}$	+1.4%/+0.3%	+0.8%/−0.1%
EOC MA mass (kg)	1094	851
Batch 8		
Pu initial	16.0%	16.6%
$\Delta Pu/\Delta Pu_{fissile}$	+1.2%/+0.2%	+0.7%/−0.0%
EOC MA mass (kg)	1135	872

IX.A. Plutonium Evolution

The low Pu CP core reaches a Pu fraction equal to the initial Pu fraction of the high Pu HS core at the beginning of batch 6, but where the CP core shows a positive ΔPu and $\Delta Pu_{fissile}$ in batch 6, the high Pu HS core shows a considerable loss of fissile material in the first batch. This difference is attributed to small spectral differences between the CP and HS core and to differences of the Pu vector, which contains more ^{240}Pu in batch 6. In batch 6 the CP core has a better conversion from ^{240}Pu to ^{241}Pu and a net increase of ^{241}Pu during the irradiation period while ^{239}Pu is almost constant. In the first batch of the high Pu HS core, there is a rapid increase in ^{240}Pu, ^{239}Pu shows a gradual decrease, and ^{241}Pu shows a rapid decrease. In Fig. 9 the Pu densities are given for the low Pu CP core in batch 6, and Fig. 10 gives the Pu density of the high Pu HS core in batch 1. Especially, the evolution of ^{241}Pu is different.

In batch 8 the Pu content of the low Pu CP core reaches the same value as the high Pu HS core in batch 5. Again, the CP core has an increase in fissile mass, and the HS core has a slight decrease from BOC to EOC, but in this case the differences are small. The differences are attributed to the difference in Pu vector, which is slightly

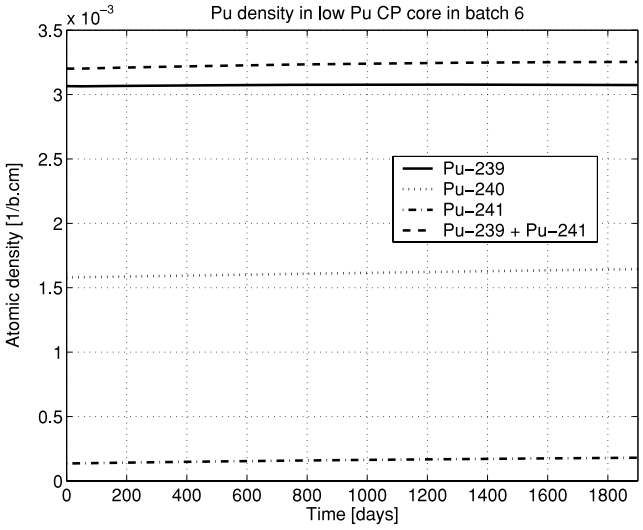

Fig. 9. Evolution of ^{239}Pu, ^{240}Pu, and ^{241}Pu in batch 6 for the low Pu CP core. The density of ^{239}Pu is almost constant during irradiation, and ^{241}Pu increases. The increase of ^{241}Pu is the cause of the overall increase of fissile material during irradiation. During the decay period 22% of the ^{241}Pu nuclei will decay, and batch 7 will start with roughly the same ^{241}Pu density as batch 6.

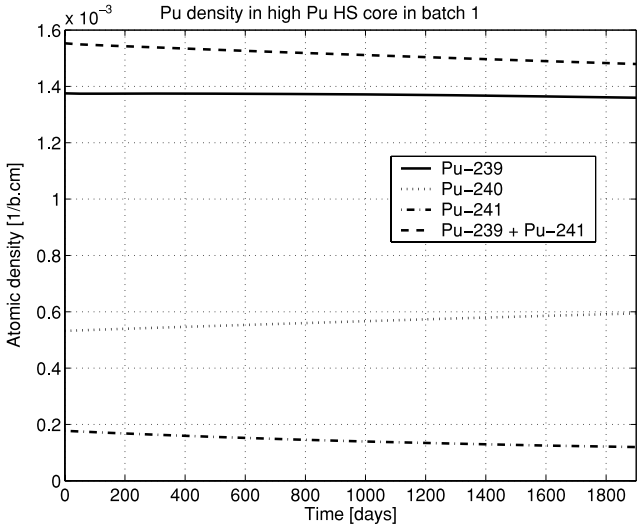

Fig. 10. Evolution of ^{239}Pu, ^{240}Pu, and ^{241}Pu in batch 1 for the high Pu HS core. The overall Pu enrichment in this case is the same as in Fig. 9, but the different Pu vector causes a different evolution. Plutonium-239 shows a decrease, and ^{241}Pu shows a rapid decrease during irradiation, with ^{240}Pu increasing rapidly. The total fissile mass decreases. During the decay period 22% of the ^{241}Pu will decay, so batch 2 starts with an even smaller amount of fissile material than indicated in this graph.

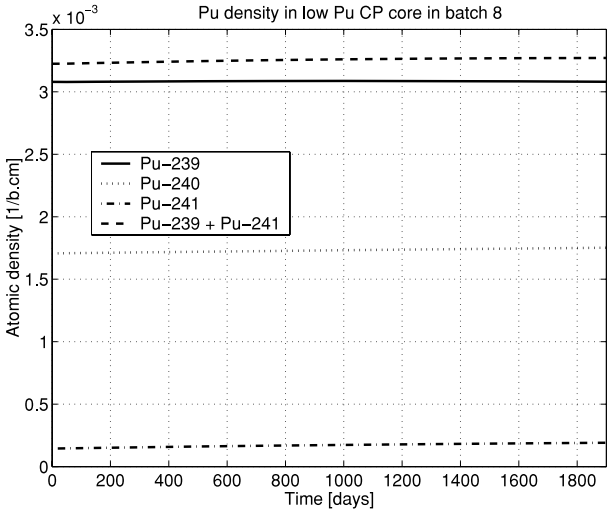

Fig. 11. Evolution of ^{239}Pu, ^{240}Pu, and ^{241}Pu in batch 8 for the low Pu CP core. The overall Pu enrichment in this case is the same as in Fig. 14. The ^{239}Pu is almost constant, as is ^{241}Pu. Also, ^{240}Pu shows a less rapid increase as in earlier batches. This seems an indication that an equilibrium is being reached.

more ^{240}Pu rich in batch 8, leading to better conversion of ^{240}Pu to ^{241}Pu. Figures 11 and 12 give the Pu density in the low Pu CP core in batch 8 and in the high Pu HS core in batch 5, respectively.

In the later fuel batches, ΔPu decreases for both cores: The total amount of Pu becomes almost constant. This is due to an equilibrium setting between ^{240}Pu production on one side and conversion of ^{240}Pu to ^{241}Pu on the other side. It seems that the equilibrium core would have ~16.5% Pu, with a large amount of ^{240}Pu.

The high Pu HS core has an almost constant density of ^{239}Pu during all batches except the first two (decrease in the first batches). During all fuel batches except the first two, the amount of ^{241}Pu increases during irradiation. During subsequent decay ~22% of ^{241}Pu decays, leading to the negative $\Delta Pu_{fissile}$ from batch to batch. However, the higher density of ^{240}Pu in the later batches leads to more ^{241}Pu production during irradiation, improving $\Delta Pu_{fissile}$. In the low Pu CP core, the ^{239}Pu density stabilizes after batch 5. The high ^{240}Pu content in the later batches leads to higher ^{241}Pu production. In the later batches $\Delta Pu_{fissile}$ decreases for the low Pu CP core, indicating that an equilibrium is reached.

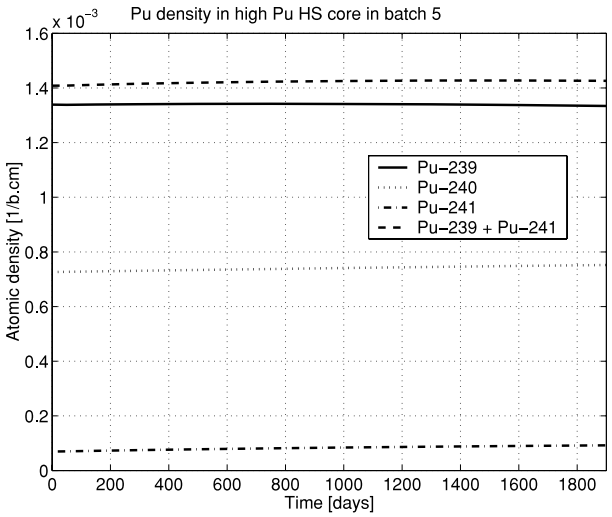

Fig. 12. Evolution of ^{239}Pu, ^{240}Pu, and ^{241}Pu in batch 5 for the high Pu HS core. The overall Pu enrichment in this case is the same as in Fig. 13. The fuel vector for this period does not differ very much from the vector in Fig. 13, and the evolution of the nuclide densities is almost the same. The ^{239}Pu is almost constant, as are ^{241}Pu and ^{240}Pu. The decay of ^{241}Pu during reprocessing still causes a smaller fissile mass at the beginning of batch 6.

IX.B. k_{eff} and FTC

For the first batch, k_{eff} of the low Pu CP core is a decreasing function, but in all subsequent batches, k_{eff} increases during irradiation. This is attributed to the increase of fissile mass after the first batch. For the high Pu HS core, k_{eff} decreases during irradiation in the first two batches, but in all subsequent batches, k_{eff} increases from

BOC, reaches a maximum sometime between 1200 and 1400 days, and then decreases again. At EOC k_{eff} is larger than at BOC and only slightly larger than 1 for the HS core. By increasing the total HM loading of the core, one can increase k_{eff}. For both cores k_{eff} at the beginning of a batch is not equal to k_{eff} at the end of the previous irradiation period because of the loss of fissile material due to decay of ^{241}Pu and because the fissile material has a different spatial distribution in the new core.

In all cases the FTC is negative. An illustration is given in Figs. 13 and 14, where k_{eff} is given for the low Pu CP core and the high Pu HS core in batch 6. The magnitude of the FTC is somewhat smaller than in the first batch, an effect caused by the presence of MAs in the fuel (see Figs. 5 and 7 for k_{eff} and FTC in the first batch).

IX.C. Minor Actinides

Upon inspection of Figs. 9, 11, and 12, it is clear that the densities of the various Pu nuclides are almost constant in the later fuel batches. This is also true for the MAs: The masses of MAs in both cores grow from batch to batch, but in the later batches, the increase per cycle is much smaller than in the first batches.

The evolutions of the Pu nuclide density in the low Pu CP core and low Pu HS core do not differ fundamentally, so it is expected that the low Pu HS core will have long-term performance similar to the low Pu CP core, with the most important difference that k_{eff} will be an increasing function for the first batch as well. The high Pu CP core has a k_{eff} below 1 for the third and fourth batches, but this can be improved by increasing the HM loading of the core. This core should have long-term performance similar to the high Pu HS core. The performance of the cores regarding MAs is also expected to not differ fundamentally between the CP design and the HS cores.

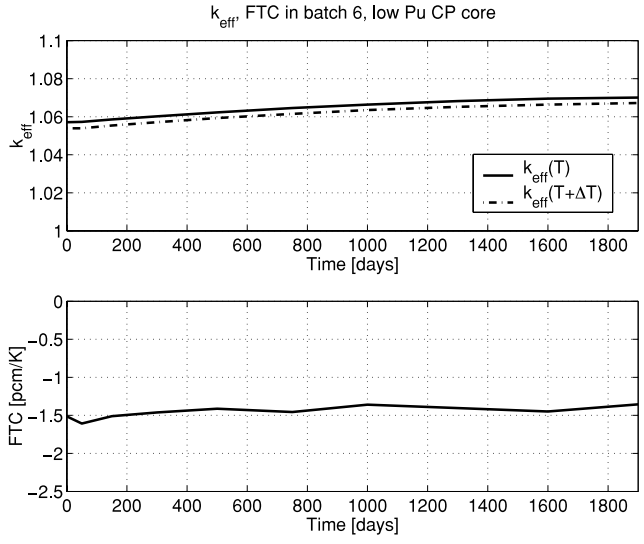

Fig. 13. The k_{eff} and FTC in batch 6, low Pu CP core. The smaller magnitude of the FTC (compare Fig. 5) is caused by the MAs in the fuel in batch 6.

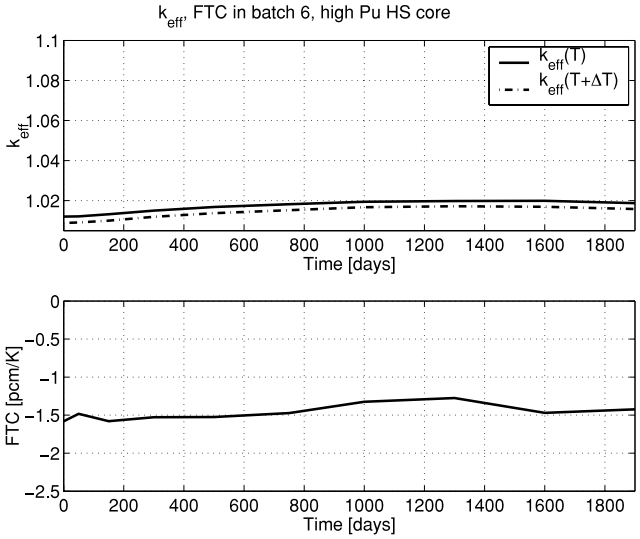

Fig. 14. The k_{eff} and FTC in batch 6, high Pu HS core.

X. CONCLUSION

The specific demands of the GCFR core with, for a gas cooled reactor, a relatively high power density, a high volume fraction of fuel, and the impossibility of using steel, requires a totally new fuel and core concept. TRISO CP fuel can be used, but a redesign of the CP is necessary to adapt it to the GCFR environment. It is difficult to apply a fuel compact of CPs embedded in a matrix because the volume fraction of fuel in the fuel compact would be (too) low and because of thermal limitations in the high-power-density GCFR core. Therefore, a core concept is chosen with direct cooling of the coated particles, with the extra advantage that the fuel temperatures will be only marginally higher than the temperature of the coolant. The application of more or less proven TRISO technology reduces research and development needs for the GCFR.

A burnup simulation was done for a 2400-MW(thermal) GCFR core, with a power density of 50 MW/m^3. The core has no blankets and uses a mix of LWR discharge Pu and ^{238}U for the first fuel loading. In the reprocessing step all TRU material is recycled in the core. The goal of a self-sustaining core, i.e., a core that produces enough new fissile material such that refueling with only a fertile material (^{238}U in this case) is sufficient, is met. Two core designs with two Pu loadings (low and high) were simulated, with an initial Pu content of

~13 and 15.5%. As expected, a lower Pu content improves Pu production from ^{238}U. In all core concepts the total Pu mass increases during irradiation, and in the low Pu cores, the fissile mass also increases during irradiation. In the high Pu cores on the other hand, the fissile mass decreases during irradiation. It is possible by adjusting the total HM loading and the Pu content to obtain a fuel composition that gives a slight increase in fissile mass during the first batches, with the increase of fissile mass becoming smaller in later batches. The resulting fuel vector will be rich in ^{239}Pu and ^{240}Pu and poor in ^{241}Pu. Calculations have shown that the Pu vector has an important influence on the evolution of the fuel. A small difference in the Pu vector can make the difference between a net consumption or production of fissile material with the same overall Pu content. All studied cores are currently below the limit of 15 tonnes Pu/GW(electric), and there is some room for optimization.

The k_{eff} is an increasing function of irradiation time or shows a maximum, especially in the later fuel batches. This means that the GCFR could be operated for a long time with a limited amount of overreactivity at BOC. The calculated values of k_{eff} are sometimes barely larger than unity, and for one core design, they are even smaller than 1, but this can be improved by enlarging the HM loading of the core. Under all circumstances the FTC is negative, with a decreasing magnitude during irradiation due to fission product buildup.

The goal of a self-sustaining core can be achieved with the GCFR concept. The resulting Pu is quite rich in ^{240}Pu, improving proliferation resistance. Only ^{238}U is added to the core during its lifetime to make the new fuel. Because all TRUs are recycled in the core, only fission products are put into the repository. Because of high-temperature output, high-efficiency power conversion is possible. All these points together make the GCFR a reactor concept that fits better into the picture of sustainable development than present reactor concepts. The presented core concepts remain within the tentative limits set on the volume fractions of fuel, coolant, and structural materials within the Generation IV roadmap.

The core layout and fuel design presented in this paper still offer many opportunities for optimization. For instance, a relatively simple material (stainless steel) has been used for the reflectors. There are several compounds, e.g., ZrSi compounds, that have better neutronic performance. The height/diameter ratio of the core can be varied. A lower core allows for a higher volume fraction of fuel elements in the core, or a more "open" core can be designed to improve natural circulation behavior or enable operation at a higher power density. The geometry of the fuel elements has various free variables, offering many possibilities for optimization. For instance, the buffer volume may be reduced because burnups beyond 5 or 6% FIMA will not be reached. A higher volume fraction of fuel per fuel element enables a more open core or a reduction of core volume.

APPENDIX

A NOTE ON FUEL ASSEMBLY DESIGN

For the CP core the particle beds should not exceed a height of ~2 or 3 cm. In a first approximation, a fuel assembly is modeled as a simple cylinder with a radius $r_{cyl} \approx 6$ cm. Within this cylinder is the particle bed, modeled as a simple right annulus of inner radius r_i and outer radius r_o. The power produced within one grid cell is simply the product of the power density times the volume of the outer cylinder and corrected for the hexagonal pitch (the fuel cylinder does not completely fill a hexagonal grid cell), and for the power peaking. If ΔT is known (or chosen to be some value), the mass flow of coolant through the fuel cylinder is known from the formula $\dot{m} = Q/c_p\Delta T$, with Q the power of the fuel cylinder. If the coolant enters the cylinder from below, and if it flows in the area between the outer cylinder and the fuel bed, the entrance area A_{in} of the coolant is known ($A_{in} = \pi(r_{cyl}^2 - r_o^2)$), as are the temperature and pressure of the cold coolant. With these numbers the flow speed of the coolant at the entrance v_{in} is given by

$$v_{in} = \frac{\dot{m}}{\rho_f(P_{in}, T_{in})A_{in}}$$

with P_{in} and T_{in} the pressure and temperature of the fluid at the entrance. The maximum speed needs to be selected (for this paper 125 m/s is assumed), and now the corresponding A_{in} can be calculated, and this gives the value of r_o of the particle bed. Using the same reasoning, the velocity of the hot gas leaving the cylinder can be calculated, and using the same maximum v, r_i of the particle bed is found using $A_{out} = \pi r_i^2$. Using the fact that the annulus is a simple straight annulus, the volume of the particle bed can be calculated as a fraction of the entire fuel cylinder ($r_{cyl}^2/(r_o^2 - r_i^2)$), and doing so the volume fractions of coolant and particles for the entire core are known. This calculation is conservative as it is based on the most highly rated fuel assembly requiring the largest mass flow of coolant. The same approach gives the dimensions of the fuel beds of the HS core.

NOMENCLATURE

A	= cross-sectional flow area
A_{in}	= coolant entrance flow section
A_{out}	= coolant exhaust flow section
c_p	= isobaric heat capacity of fluid
d_p	= diameter of spherical particle
FTC_{max}	= maximum value of FTC
FTC_{min}	= minimum value of FTC
h_c	= height of core

k = Boltzmann's constant

k_{eff} = effective core multiplication factor

k_{max} = maximum value of k_{eff}

k_{min} = minimum value of k_{eff}

L = packed bed height

$\dot{m}$ = mass flow rate

ΔMA = change in mass of MA isotopes

n_0 = initial number of HM atoms in the fuel kernel

ΔP = pressure difference

P_{buf} = buffer pressure

P_{in} = coolant pressure at inlet

ΔP_{pb} = pressure drop over packed bed

ΔPu = change in mass of all Pu isotopes

$\Delta \text{Pu}_{fissile}$ = change in mass of fissile Pu isotopes

Q = power produced by a fuel cylinder

$\bar{Q}$ = average power density

Q_p = power produced by a pebble

R = shell radius

r_b = radius of TRISO buffer

r_c = radius of core

r_{cyl} = radius of fuel cylinder

r_{fz} = radius of the fuel zone

r_i = inner radius of fuel cylinder

r_k = radius of TRISO fuel kernel

r_o = outer radius of fuel cylinder

r_t = radius of entire TRISO particle

ΔT = temperature rise over packed bed

T_{buf} = temperature of the buffer

ΔT_p = temperature difference between center and surface of fuel pebble

T_{in} = coolant temperature at inlet

T_{out} = coolant temperature at outlet

T_0 = nominal operating temperature

ΔT_0 = temperature increase to calculate FTC

u = superficial fluid velocity

V_{buf} = free volume of the buffer

v_{in} = coolant flow speed at entrance

z = number of gas atoms released from fuel per fissioned metal atom

Greek

δ = shell thickness

ϵ = packed bed porosity

λ = heat conductivity of graphite mixture

μ_f = fluid viscosity

ρ_f = density of fluid

σ_{ii} = tangential stress in shell

σ_{max} = maximum (rupture) stress

REFERENCES

1. G. MELESE and R. KATZ, *Thermal and Flow Design of Helium-Cooled Reactors*, American Nuclear Society, La Grange Park, Illinois (1984).

2. A. TORRI and D. R. BUTTEMER, "Gas-Cooled Fast Reactor Safety—An Overview and Status of the U.S. Program," *Proc. Gas-Cooled Reactor Safety and Licensing Aspects (IWGCR-1)*, Lausanne, Switzerland, September 1–3, 1981, p. 51, International Atomic Energy Agency (1981).

3. H. MOCHIZUKI, T. IZAKI, K. TAKITANI, H. KOIKE, Y. KOBAYASHI, Y. MATSUKI, T. OOKA, R. TANAKA, T. WATANABE, and T. KOBAYASHI, "Design Study of a Gas-Cooled Fast Breeder Reactor," *Proc. Gas-Cooled Fast Reactors*, Minsk, USSR, July 24–28, 1972, IAEA-TECDOC-154, International Atomic Energy Agency (1972).

4. A. E WALTAR and A. B REYNOLDS, *Fast Breeder Reactors*, Pergamon Press, New York (1981).

5. A. M. SUKHOTIN, N. Ya. LANTRATOVA, V. P. TRUBNIKOV, and Eh. I. ATROSHENKO, "Coolant Technology and Corrosion Stability of Construction Materials in N_2O_4," *Proc. Gas-Cooled Fast Reactors*, Minsk, USSR, July 24–28, 1972, IAEA-TECDOC-154, International Atomic Energy Agency (1972).

6. V. B NESTERENKO, V. F. ZELENSKY, L. I. KOLYKHAN, G. V. KARPENKO, V. S. KRASNORUTSKY, V. P. ISAKOV, V. P. ASHIKHMIN, and L. N. PERMYAKOV, "Problems of Creating Fuel Elements for Fast Gas-Cooled Reactors Working on N_2O_4-Dissociating Coolant," *Proc. Gas-Cooled Reactor Fuel Development and Spent Fuel Treatment (IWGGCR-8)*, Moscow, Russian Federation, October 18–21, 1983, International Atomic Energy Agency (1983).

7. J. CHERMANNE, "GCFR Fuel Assemblies," *Proc. Gas-Cooled Fast Reactors*, Minsk, USSR, July 24–28, 1972, IAEA-TECDOC-154, International Atomic Energy Agency (1972).

8. J. CHERMANNE, "GCFR Safety," *Proc. Gas-Cooled Fast Reactors*, Minsk, USSR, July 24–28, 1972, IAEA-TECDOC-154, International Atomic Energy Agency (1972).

9. J. CHERMANNE and P. BERGSMÜLLER, "Gas-Cooled Breeder Reactor Safety," *Proc. Gas-Cooled Reactor Safety and*

Licensing Aspects (IWGGCR-1), Lausanne, Switzerland, September 1–3, 1981, International Atomic Energy Agency (1981).

10. "A Technology Roadmap for Generation IV Nuclear Energy Systems," GIF-002-00, U.S. DOE Nuclear Energy Research Advisory Committee and the Generation IV International Forum; available on the Internet at http://gif.inel.gov/roadmap/ (Dec. 2002).

11. M. COMETTO, P. WYDLER, and R. CHAWLA, "A Comparative Physics Study of Alternative Long-Term Strategies for Closure of the Nuclear Fuel Cycle," *Ann. Nucl. Energy*, **31**, 413 (2004).

12. E. A. HOFFMAN and W. M. STACEY, "Comparative Fuel Cycle Analysis of Critical and Subcritical Fast Reactor Transmutation Systems," *Nucl. Technol.*, **144**, 83 (2003).

13. M. INOUE, K. ONO, T. FUJIOKA, K. SATO, and T. ASAGA, "Feasibility Study on Nitrogen-15 Enrichment and Recycling System for Innovative FR Cycle Systems with Nitride Fuel," *Proc. 10th Int. Conf. Nuclear Engineering (ICONE 10)*, Arlington, Virginia, April 14–18, 2002, American Society of Mechanical Engineers (2002).

14. K. VERFONDERN, J. SUMITA, S. UETA, and K. SAWA, "Modeling of Fuel Performance and Metallic Fission Product Release Behavior During HTTR Normal Operating Conditions," *Nucl. Eng. Des.*, **210**, 210 (2001).

15. C. TANG, Y. TANG, J. ZHU, Y. ZOU, J. LI, and X. NI, "Design and Manufacture of the Fuel Element for the 10 MW High Temperature Gas-Cooled Reactor," *Nucl. Eng. Des.*, **218**, 91 (2002).

16. H. J. RUETTEN and J. C. KUIJPER, "Plutonium (1st and 2nd Generation) Cell Burnup Benchmark Specification," HTR-N1-02/06-s-3.1.1, European Commission (2003).

17. K. RYU and H. SEKIMOTO, "A Possibility of Highly Efficient Uranium Utilization with a Pebble Bed Fast Reactor," *Ann. Nucl. Energy*, **27**, 1139 (2000).

18. K. KUGELER and R. SCHULTEN, *Hochtemperaturreaktortechnik*, Springer-Verlag, Berlin, Germany (1989).

19. D. KINII and O. LEVENSPIEL, "Fluidized Reactor Models. 1. For Bubbling Beds of Fine, Intermediate and Large Particles. 2. For the Lean Phase: Freeboard and Fast Fluidization," *Ind. Chem. Eng. Res.*, **29**, 1226 (1991).

20. M. KONOMURA, T. SAISUGA, T. MIZUNO, and Y. OHKUBO, "A Promising Gas-Cooled Fast Reactor Concept and Its R&D Plan," *Proc. Global 2003*, New Orleans, Louisiana, November 16–20, 2003, American Nuclear Society (2003) (CD-ROM).

21. "SCALE-4.2 Modular Code System for Performing Standardized Computer Analyses for Licensing Evaluations," Oak Ridge National Laboratory (1994).

22. J. E. HOOGENBOOM and J. L. KLOOSTERMAN, "Generation and Validation of ORIGEN-S Libraries for Depletion and Transmutation Calculations Based on JEF-2.2 and EAF3 Basic Data," *Nucl. Eng. Des.*, **170**, 107 (1997).